Rapid Prototyping of Patterned Functional Nanostructures

Hongyou Fan[‡], Yunfeng Lu[‡], Aaron Stump[‡], Scott T. Reed[†], Tom Baer[†], Randy, Schunk, Victor Perez-Luna[‡], Gabriel P. López[‡], and C. Jeffrey Brinker[†‡]

[‡]The University of New Mexico Center for Micro-Engineered Materials and [†]Department of Chemical and Nuclear Engineering, Albuquerque, NM 87131.
Sandia National Laboratories, Albuquerque, NM, 87185.

Living systems exhibit form and function on multiple length scales, and the prospect of imparting life-like qualities to man-made materials has inspired many recent efforts to devise hierarchical materials assembly strategies. For example, Yang et al.[1] grew surfactant-templated mesoporous silica[2] on hydrophobic patterns prepared by micro-contact printing μCP[3]. Trau et al.[4] formed oriented mesoporous silica patterns, using a micro-molding in capillaries $MIMIC$ technique[3], and Yang et al.[5] combined $MIMIC$, polystyrene sphere templating[6], and surfactant-templating to create oxides with three levels of structural order. Overall, great progress has been made to date in controlling structure on scales ranging from several nanometers to several micrometers. However, materials prepared have been limited to oxides with no specific functionality, whereas for many of the envisioned applications of hierarchical materials in micro-systems, sensors, waveguides, photonics, and electronics, it is necessary to define both form and function on several length scales. In addition, the patterning strategies employed thus far require hours or even days for completion[1, 4, 5]. Such slow processes are inherently difficult to implement in commercial environments.

We have combined evaporation-induced (silica/surfactant) self-assembly $EISA$[7] with rapid prototyping techniques like pen lithography[8, 9], ink-jet printing[10, 11], and dip-coating on micro-contact printed substrates to form hierarchically organized structures in seconds. In addition, by co-condensation of tetrafunctional silanes $(Si(OR)_4)$ with tri-functional organosilanes $((RO)_3SiR')$[12-14] or by inclusion of organic additives, we have selectively derivatized the silica framework with functional R' ligands or molecules. The resulting materials exhibit form and function on multiple length scales: on the molecular scale, functional organic moieties are positioned on pore surfaces, on the mesoscale, mono-sized pores are organized into 1-, 2-, or 3-dimensional networks, providing size-selective accessibility from the gas or liquid phase, and on the macroscale, 2-dimensional arrays and fluidic or photonic systems may be defined.

Scheme 1 (Figure 1) schematically illustrates direct writing of a mesoscopically ordered nanostructure, using micro-pen lithography MPL.[9] For ink we use homogeneous solutions of

DISCLAIMER

DISCLAIMER

Portions of this document may be illegible
in electronic image products. Images are
produced from the best available original
document.

TEOS, ethanol, water, surfactant, acid, and (optionally) organosilanes and other organic ingredients (see Table 1). These solutions are prepared with an initial surfactant concentration c_o less than the critical surfactant concentration cmc and an acid concentration designed to minimize the siloxane condensation rate, thereby enabling facile silica/surfactant self-assembly within the brief time span of the writing operation. As the ink is metered onto the surface, preferential ethanol evaporation causes enrichment of water, surfactant, and silica, establishing a 3-D (longitudinal and radial) gradient in their respective concentrations (Figure 1). Where cmc is exceeded, cooperative silica/surfactant self-assembly creates micelles. Further evaporation, of predominantly water, promotes the continuous self-organization of micelles into silica/surfactant liquid crystalline mesophases. As demonstrated previously for *EISA* of films[15] and aerosols[16], liquid crystalline domains are nucleated by incipient surfactant monolayers formed at solid-liquid[17, 18] and liquid-vapor interfaces[19] (at $c < cmc$) and grow inward as evaporation proceeds.

Figure 2a shows a meandering macroscopic pattern formed in several seconds by *MPL* of a rhodamine B-containing solution on a hydrophilic surface (hydroxylated native oxide of <100> silicon). The inset in Figure 2a shows the corresponding fluorescence image of several adjacent stripes, and the TEM micrograph (Figure 2c) reveals the ordered pore structure characteristic of a cubic thin film mesophase. The *MPL* line width can vary from micrometers to millimeters. It depends on such factors as pen dimension[8], wetting characteristics, evaporation rate, capillary number (Ca = ink viscosity x substrate speed/surface tension) and ratio of the rates of ink supply and withdrawal (inlet velocity/substrate velocity). The effect of wetting has been demonstrated by performing *MPL* on substrates pre-patterned with hydrophobic, hydrophilic or mixed SAMs. Generally, line widths are reduced by increasing the contact angle and by reducing the inlet/substrate velocity ratio. The conditions providing the minimum stable line width are bounded by a regime of capillary instability – we anticipate that this instability could be exploited to create periodic arrays of dots.

The advantages of *MPL* are that we can use computer-aided design to define any arbitrary 2-D pattern and that we can use any desired combination of surfactant and functional silane as ink to selectively define different functionalities at different locations. However *MPL* is a serial technique. In situations where it is desirable to create an entire pattern with the same functionality, it would be preferable to employ a parallel technique in which the deposition process occurred simultaneously in multiple locations. Scheme 2 (Figure 3) illustrates a rapid, parallel patterning procedure, dip-coating on patterned SAMs. This procedure uses micro-contact printing[20] or electrochemical patterning[21] of hydroxyl- and methyl-terminated SAMs to define hydrophilic and hydrophobic patterns on the substrate surface. Then using homogenous solutions identical to those employed for *MPL*, preferential ethanol evaporation during dip-coating enriches the depositing film in water, causing *selective de-wetting* of the hydrophobic regions. In this fashion, lines, arrays of dots, or other arbitrary shapes can be deposited on

hydrophilic patterns in seconds. As described for *MPL*, further evaporation accompanying the dip-coating operation induces self-assembly of silica/surfactant mesophases.

The patterned dip-coating procedure may be conducted with organic dyes or functional silanes (see Table 1). Scheme 2 illustrates patterned deposition of a propyl-amine derivatized cubic mesophase followed by a conjugation reaction with a pH-sensitive dye, 5,6-carboxyfluorescein, succinimidyl ester (5,6-FAM, SE). The uniform continuous porosity of the amine-derivatized and dye-conjugated films is confirmed by TEM and surface acoustic wave (SAW)-based nitrogen sorption isotherms[22] of the corresponding films deposited on SAW substrates (Figure 4). The reduction in film porosity after dye conjugation reflects the volume occupied by the attached dye moieties. The patterned, functional array can be used to monitor the pH of fluids introduced at arbitrary locations and transported by capillary flow into the imaging cell. Figure 4a shows the fluorescence image of an array contacted with three different aqueous solutions prepared at pH 4.8, 7.7, and 12.0. Figure 4b shows the corresponding emission spectra and provides a comparison with solution data. In combination, the fluorescence image (Fig. 4a) and plan-view and cross-sectional TEM micrographs (Figures 3 and 4c) of the dye-conjugated film demonstrate the uniformity of macro- and mesoscale features achievable by this evaporation-induced, de-wetting and self-assembly route. In comparison, films formed by nucleation and growth of thin film mesophases on patterned SAMs[1] are observed to have non-homogeneous, globular morphologies.

Finally we can create patterned nanostructures by combining *EISA* with a variety of aerosol processing schemes. For example, Figure 5 compares an optical micrograph of a macroscopic array of spots formed by ink jet printing *IJP*[10, 11]on a silicon wafer with *IJP* of standard ink on a non-adsorbent surface. The *IJP* process dispenses the *ink* (prepared as for *MPL*) as monosized, spherical aerosol droplets. Upon impaction the droplets adopt a new shape that balances surface and interfacial energies. Accompanying evaporation creates within each droplet a gradient in surfactant concentration that that drives radially-directed silica/surfactant self-assembly inward from the liquid-vapor interface[16]. The inset in Figure 5 shows a representative TEM micrograph of a hydrophobic, fluoroalkylated silica mesophase formed by *IJP*. The resolution achieved compared to standard ink and our ability to selectively functionalize the ink suggest applications in display technologies. Continuous, nanostructured lines are created by coalescence of overlapping droplets. Patterns may also be created by aerosol deposition through a mask or by aerosol deposition on patterned hydrophilic/hydrophobic surfaces (H. Fan, Y. Lu, and A. Stump, unpublished).

Methods

Precursor solutions used as inks were prepared by addition of surfactants (cationic, CTAB; $CH_3(CH_2)_{15}N^+(CH_3)_3Br^-$ or non-ionic, Brij-56; $CH_3(CH_2)_{15}-(OCH_2CH_2)_{10}-OH$), organosilanes

(R'Si(OR)₃, see Table 1), or organic molecules (see Table 1) to an acidic silica sol (A2**). The acid concentration employed in the A2** synthesis procedure was chosen to minimize the siloxane condensation rate, thereby promoting facile self-assembly during writing, printing, etc[15]. In a typical preparation, TEOS [$Si(OCH_2CH_3)_4$], ethanol, water and dilute HCl (mole ratios: $1:3.8:1:5\times10^{-5}$) were refluxed at 60 °C for 90 min. The sol was diluted with 2 volumes of ethanol followed by further addition of water and HCl. Organosilanes (R'-Si(OR)₃, where R' is a non-hydrolyzable organic functional ligand) were added followed by surfactants and (optionally) organic additives (see Table 1). Surfactants were added in requisite amounts to achieve initial surfactant concentrations c_0 ranging from 0.004 to 0.23 M ($c_0^{'} \ll cmc$). The final reactant molar ratios were: 1 TEOS : 22 C_2H_5OH : 5 H_2O : 0.093 – 0.31 surfactant : 0.039 – 0.8 organosilanes : 2.6×10^{-5} organic additives. It should be noted that co-hydrolysis of organosilanes with TEOS in the initial A2** sol preparation, generally resulted in disordered worm-like mesostructures[23]. After pattern deposition and drying, the surfactant templates were selectively removed by calcination in a nitrogen atmosphere at a temperature sufficient to decompose the surfactant molecules (e.g., 350 °C) without degrading the covalently-bound organic ligands or by solvent extraction.

Patterning Procedures

Micropen lithography was performed using a Model 400a micropen instrument purchased from Ohmcraft Inc., Pittsford, NY. The pen orifice was 50 μm and the writing speed was 2.54 cm/s. The pattern was designed using AutoCAD 14 software.

Dip-coating of patterned (hydrophilic/hydrophobic) substrates was performed at a withdrawal speed of 7.6 — 51 cm/min under ambient laboratory conditions. Hydrophilic/hydrophobic patterns were created by microcontact printing of hydrophobic, n-octadecyltrichlorosilane ($CH_3(CH_2)_{17}SiCl_3$) self-assembled monolayers *SAMs*[24] on hydrophilic silicon substrates (hydroxylated native oxide) or by a technique involving electrochemical desorption of a hydroxyl-terminated *SAM* prepared from 11-mercaptoundecanol ($HO(CH_2)_{11}SH$) from patterned, electrically isolated gold electrodes followed by immersion in a 1 mM ethanolic solution of 1-dodecanethiol, $CH_3(CH_2)_{11}SH$[21].

Ink jet printing was performed using a Model HP DeskJet 1200C printer purchased from Hewlett-Packard Co., San Diego, CA. The pattern was designed using Microsoft PowerPoint 98 software.

Figure 1. Scheme 1: micro-pen lithography *MPL* of a surfactant-templated mesophase. a) Simulation of 3-D, binary fluid pattern dispensed on a flat substrate with substrate speed = 2.54 cm/s and fluid injection rate (inlet velocity) = 3.985 cm/s. Color contours represent evaporation-induced, 3-D gradients in alcohol-composition. Fluid was modeled as 54 volume % ethanol and

46 volume % non-volatile phase with Reynolds number = 1.25 and Ca = 0.000833. An ad hoc value of 45° was chosen for the static contact angle. Note that this angle persists at all points on the dynamic contact line because of the dominance of surface tension at this low value of Ca. b) The initially homogeneous sol metered on to the moving substrate experiences preferential evaporation of alcohol creating a complex 3-D (longitudinal and radial) gradient in the concentrations of water and non-volatile surfactant and silicate species. Progressive enrichment of silica and surfactant induces micelle formation and subsequent growth of silica/surfactant mesophases inward from solid-liquid and liquid-vapor interfaces as recently demonstrated for thin films[15] and aerosols[16]. The numerical method utilized for (a) and (b) consisted of a 3D finite element discretization of the Navier Stokes equations augmented with a three dimensional boundary-fitted mesh motion algorithm to track the free surface[25, 26]. Special relations at the 3D dynamic wetting line were also applied.

Figure 2. Meandering patterned mesophase created by *MPL*.   a) Optical micrograph of patterned rhodamine-B containing silica mesophase deposited on an oxidized [100]-oriented silicon substrate at a speed of 2.54 cm/s. Inset is a fluorescence image of rhodamine-B emission acquired through a 610-nm band pass filter, demonstrating retention of rhodamine-B functionality. b) Representative TEM micrograph of a fragment of the patterned rhodamine-B containing film corresponding to a [110]-oriented cubic mesophase with lattice constant $a =$ 10.3-nm. The sol was prepared by adding 0.01wt% rhodamine-B to a silica/4wt% Brij-56 sol. The TEOS:EtOH:water:HCl:Brij-56:rhodamine-B molar ratio = $1:22:5.0:0.004:0.075:2.6\times10^{-5}$.

Figure 3. Scheme 2: Patterned functional mesostructure formed by selective de-wetting. Using micro-contact printing or electrochemical desorption techniques, substrates are prepared with patterns of hydrophilic, hydroxyl-terminated SAMs and hydrophobic methyl-terminated SAMs. Preferential ethanol evaporation during dip-coating (1), causes water enrichment and selective de-wetting of the hydrophobic SAMs. Correspondingly film deposition occurs exclusively on the patterned hydrophilic SAMs. The sol was prepared by adding aminopropyltrimethoxysilane ($NH_2(CH_2)_3Si(OCH_3)_3$, APS) to a silica/4wt% Brij-56 sol, resulting in a final molar ratio TEOS:APS:EtOH:water:HCl:Brij-56 = 1:0.8:22:5.0:0.011:0.075. Selective de-wetting followed by calcination results in a patterned, amine-functionalized, cubic mesoporous film as is evident from the plan-view TEM micrograph (Inset A), showing a [100]-oriented cubic mesophase with $a =$ 10.3-nm and nitrogen adsorption-desorption isotherm (Inset B, curve a) acquired for the thin film specimen using a surface acoustic wave[22] (SAW) technique. The dye conjugation reaction (2) was conducted by immersion in a 0.00002mM solution of 5,6-FAM, SE (Table 1) prepared in dimethylsulfoxide (DMSO) followed by exhaustive, successive washing in DMSO, ethanol, and water. The SAW-based nitrogen adsorption-desorption isotherm of the dye-conjugated

mesoporous film is shown in Inset B, curve b, confirming its pore accessibility. BET analyses of the sorption isotherms indicate that the dye conjugation reaction reduces the surface area from 750 to 545 m^2/g and the hydraulic radius from 2.2 to 2.1-nm, but pore accessibility is completely retained as evident from combined TEM, SAW, and fluorescent-imaging results (Figure 4a).

Figure 4. Patterned pH-sensitive fluidic system. a) Fluorescence image of three adjacent 5,6-FAM, SE-conjugated pore channel networks after introduction of aqueous solutions prepared at pH 4.8, 7.7, or 12.0. Patterned dye-conjugated thin film mesophases were prepared according to Scheme 2 (Figure 3). Aqueous solutions of varying pH were introduced on the terminal pads (Figure 3) and transported into the imaging cell by capillary flow. Image was acquired using a Nikon Diaphot 300 inverted microscope and 520-nm band pass filter. b) Fluorescence spectra of 5,6-FAM, SE-conjugated mesoporous films upon exposure to aqueous solutions of pH 4.8, 7.7, and 12.0. Shown for comparison are fluorescence spectra of 0.1 micromolar solutions of 5,6-FAM, SE prepared in aqueous solutions of pH 4.8, 7.7, and 12.0. The similarity of the two sets of spectra confirms the maintenance of dye functionality upon conjugation within the mesoporous channel system. c) Cross-sectional TEM micrograph of the patterned, dye-conjugated thin film mesophase, providing evidence of the 3-D pore channel network.

Figure 5. Patterned dot arrays created by ink-jet printing. a) Optical micrograph of dot array created by ink jet printing of standard ink (from Hewlett-Packard Co., San Diego, CA) on a non-adsorbent surface. b) Optical micrograph of an array of hydrophobic, mesoporous silica dots created by evaporation-induced silica/surfactant self-assembly during *IJP* on an oxidized [100]-oriented silicon substrate followed by calcination. c) Representative TEM micrograph of a dot fragment prepared as in (b). The sol was prepared with molar ratio TEOS:TFTS(1):EtOH:water:HCl:Brij-56 = 1:0.05:22.0:5.0:0.004:0.075. The dot pattern used in a) and b) was designed using Microsoft PowerPoint 98 software. The printing rate was approximately 80 dots/s and printer resolution 300 dots/inch. The resolution achieved compared to standard ink and our ability to selectively functionalize the ink suggest applications in display technologies.

References

1. Yang, H., Coombs, N. & Ozin, G.A. Mesoporous silica with micrometer-scale designs *Adv. Mater.* **9**, 811-814 (1997).

2. Kresge, C., Leonowicz, M., Roth, W., Vartuli, C. & Beck, J. Ordered mesoporous molecular sieves synthesized by a liquid-crystal template mechanism *Nature* **359**, 710-712 (1992).

3. Xia, Y. & Whitesides, G.M. Soft lithography *Angew. Chem. Int. Ed.* **37**, 550-575 (1998).

4. Trau, M., *et al.* Microscopic patterning of orientated mesoscopic silica through guided growth *Nature* **390**, 674-676 (1997).

5. Yang, P., *et al.* Hierarchically ordered oxides *Science* **282**, 2244-2246 (1998).

6. Antonietti, M., Berton, B., Goltner, C. & Hentze, H.P. Synthesis of mesoporous silica with large pores and bimodal pore-size distribution by templating of polymer latices *Adv. Mater.* **10**, 154 (1998).

7. Brinker, C.J., Lu, Y., Sellinger, A. & Fan, H. Evaporation-induced self-assembly: nanostructures made easy *Adv. Mater.* **11**, 579-585 (1999).

8. Piner, R.D., Zhu, J., Xu, F., Hong, S. & Mirkin, C.A. "Dip-pen" nanolithography *Science* **283**, 661-663 (1999).

9. Yang, P., *et al.* Direct-write precision resistors for ceramic packages *Mat. Res. Soc. Symp. Proc.* **542**, 159-164 (1999).

10. Chang, S.-C., *et al.* Multicolor organic light-emitting diodes processed by hybrid inkjet printing *Adv. Mater.* **11**, 734-737 (1999).

11. Pede, D., Serra, G. & De Rossi, D. Microfabrication of conducting polymer devices by ink-jet stereolithography *Mat. Sci. and Eng.* **C5**, 289-291 (1998).

12. Burkett, S.L., Sims, S.D. & Mann, S. Synthesis of hybrid inorganic-organic mesoporous silica by co-condensation of siloxane and organosiloxane precursors *Chem. Commun.*, 1367-1368 (1996).

13. Fowler, C.E., Burkett, S.L. & Mann, S. Synthesis and characterization of ordered organo-silica-surfactant mesophases with functionalized MCM-41-type architecture *Chem. Commun.*, 1769-1770 (1997).

14. Lim, M.H., Blanford, C.F. & Stein, A. Synthesis and characterization of a reactive vinyl-functionalized MCM-41: Probing the internal pore structure by a bromination reaction *J. Am. Chem. Soc.* **119**, 4090-4091 (1997).

15. Lu, Y., *et al.* Continuous formation of supported cubic and hexagonal mesoporous films by sol-gel dip-coating *Nature* **389**, 364-368 (1997).

16. Lu, Y., *et al.* Aerosol-assisted self-assembly of spherical, silica nanoparticles exhibiting hexagonal, cubic, and vesicular mesophases *Nature* **398**, 223-226 (1999).

17. Aksay, I.A. Biomimetic pathways for assembling inorganic thin films *Science* **273**, 892-898 (1996).

18. Yang, H., Kuperman, A., Coombs, N., Mamiche-Afara, S. & Ozin, G.A. Synthesis of oriented films of mesoporous silica on mica *Nature* **379**, 703-705 (1996).

19. Yang, H., Coombs, N., Sokolov, I. & Ozin, G.A. Free-standing and oriented mesoporous silica films grown at the air-water interface *Nature* **381**, 589-592 (1996).

20. Wilbur, J.L., Kumar, A., Biebuyck, H.A., Kim, E. & Whitesides, G.M. Microcontact printing of self-assembled monolayers: applications in microfabrication *Nanotechnology* **7**, 452-457 (1996).

21. Tender, L.M., R.L., W., Fan, H. & Lopez, G.P. Electrochemical patterning of self-assembled monolayers onto microscopic arrays of gold electrodes fabricated by laser ablation *Langmuir* **12**, 5515-5518 (1996).

22. Frye, G.C., Ricco, A.J., Martin, S.J. & Brinker, C.J. in *Better Ceramics Through Chemistry III* (eds. Brinker, C.J., Clark, D.E. & Ulrich, D.R.) 349-354 (Mat. Res. Soc., Reno, Nevada, 1988).

23. Tanev, P.T. & Pinnavaia, T.J. A neutral templating route to mesoporous molecular-sieves *Science* **267**, 865-867 (1995).

24. Bain, C.D., *et al.* Formation of monolayer films by the spontaneous assembly of organic thiols from solution onto gold *J. Am. Chem. Soc.* **111**, 321-335 (1989).

25. Cairncross, R.A., Schunk, P.R., Baer, T.A., Rao, R.R. & Sackinger, P.A. A finite elemenet method for free-surface flows of incompressible fluids in three dimensions, Part 1: boundary-fitted mesh motion *Int. J. Numer. Meth. Fluids* in press.

26. Baer, T.A., Cairncross, R.A., Schunk, P.r., Rao, R.R. & Sackinger, P.A. A finite element method for free-surface flows of incompressible fluids in three dimensions, Part 2: Dynamic wetting lines *Int. J. Numer. Meth. Fluids* in press.

Scheme 1

(b)

pen orifice

SUBSTRATE DIRECTION

1

2

3

$C_0 \ll cmc$

Section 1

Section 2

Section 3

(a)

Volume Fraction
Ethanol
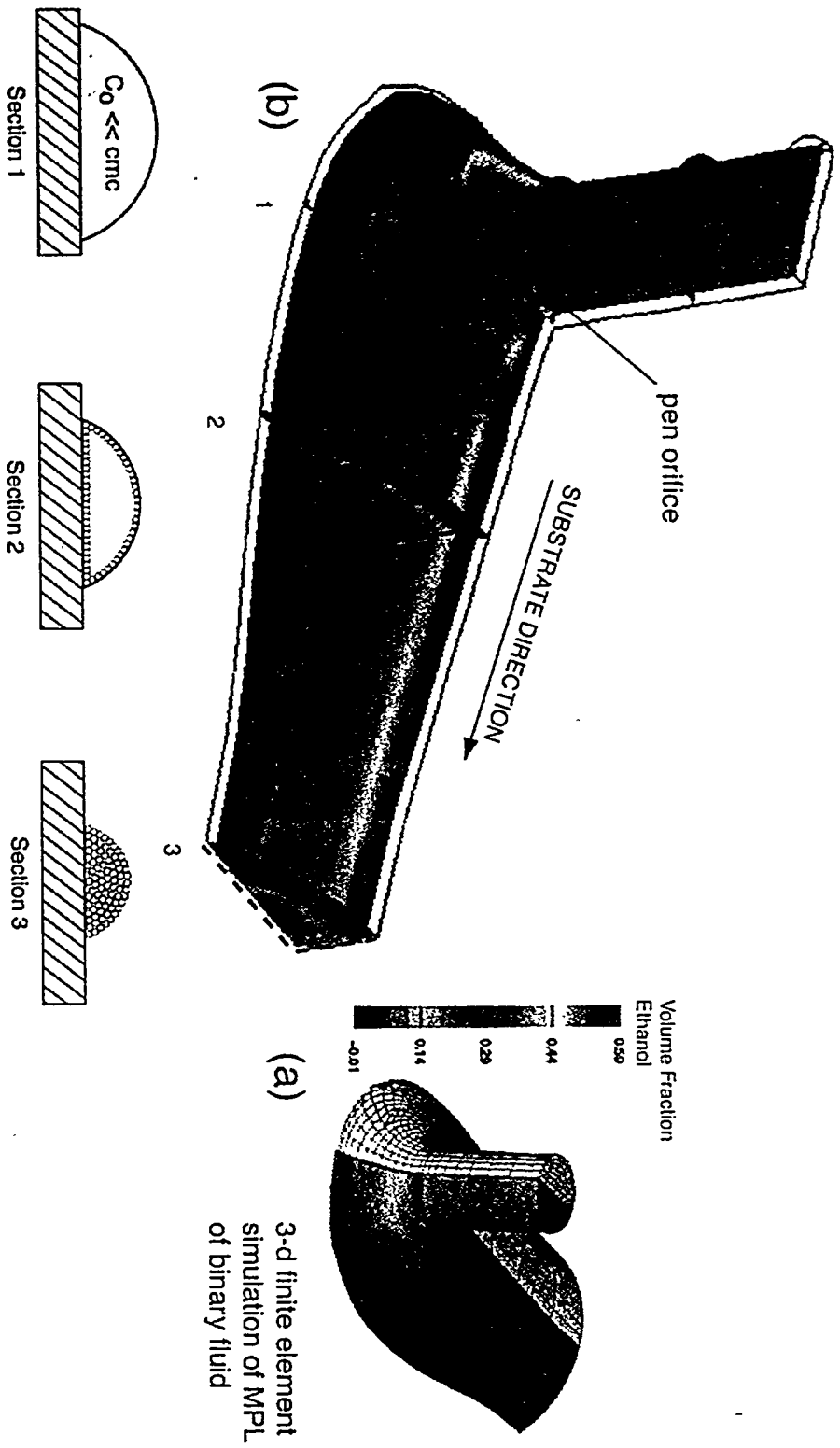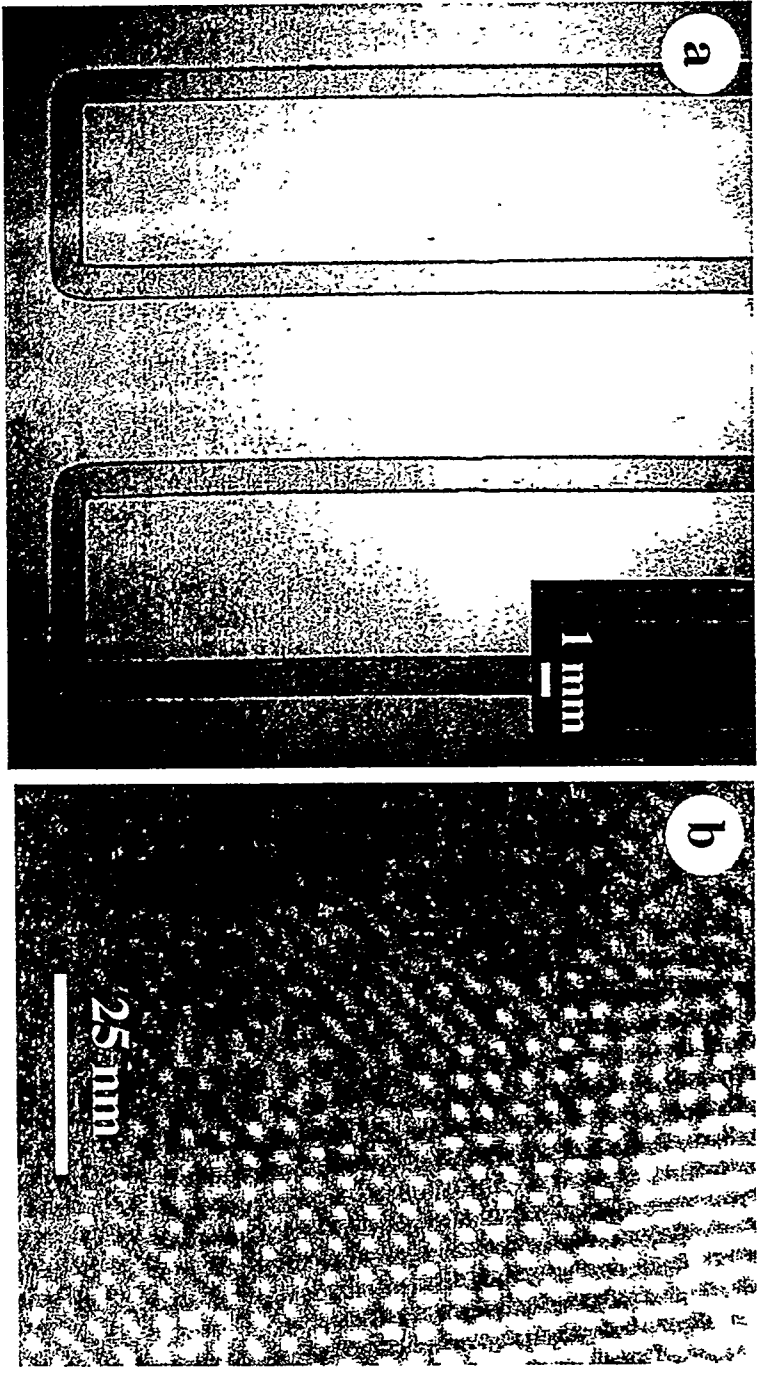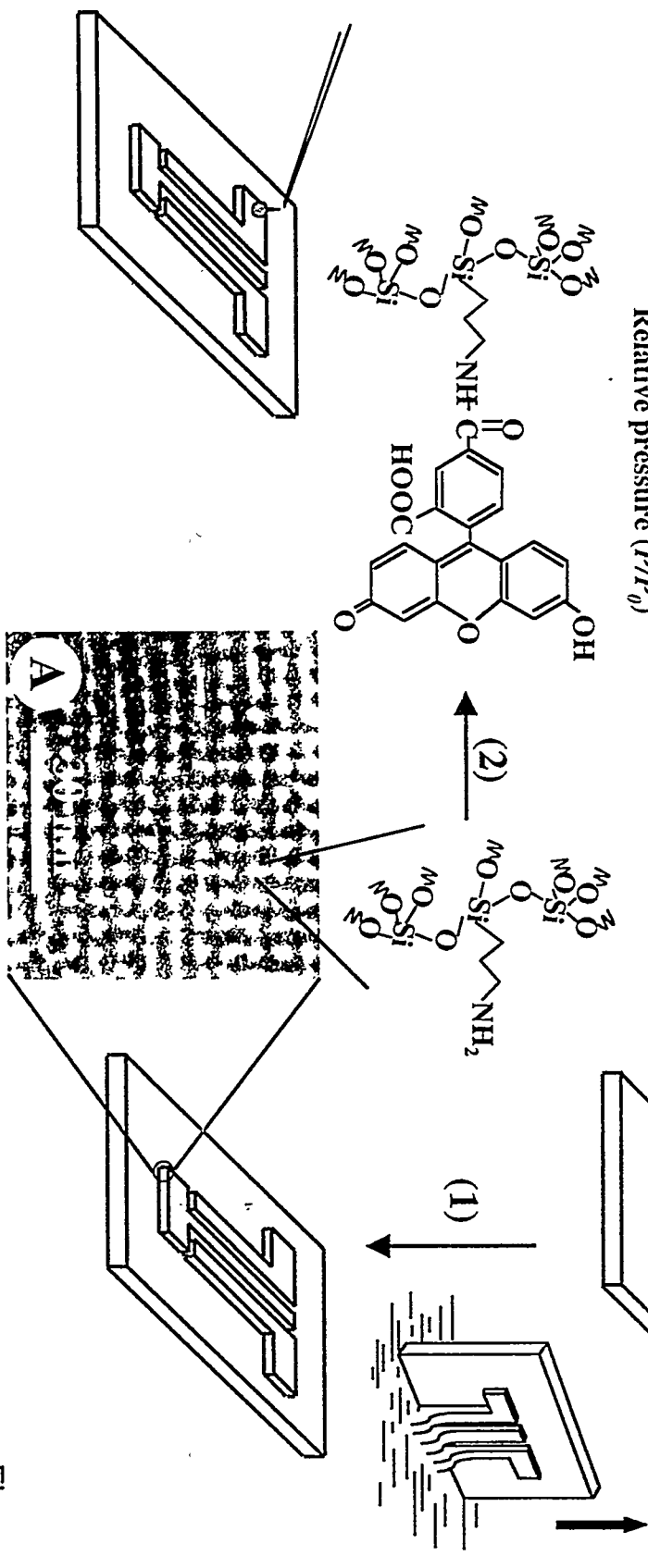
0.50

0.44

0.29

0.14

-0.01

3-d finite element
simulation of MPL
of binary fluid

Figure 1

Figure 2

Scheme 2

Figure 3

a

b
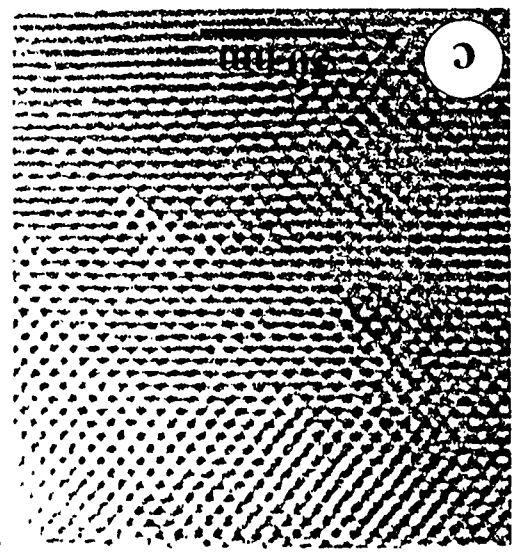
3 mm

c

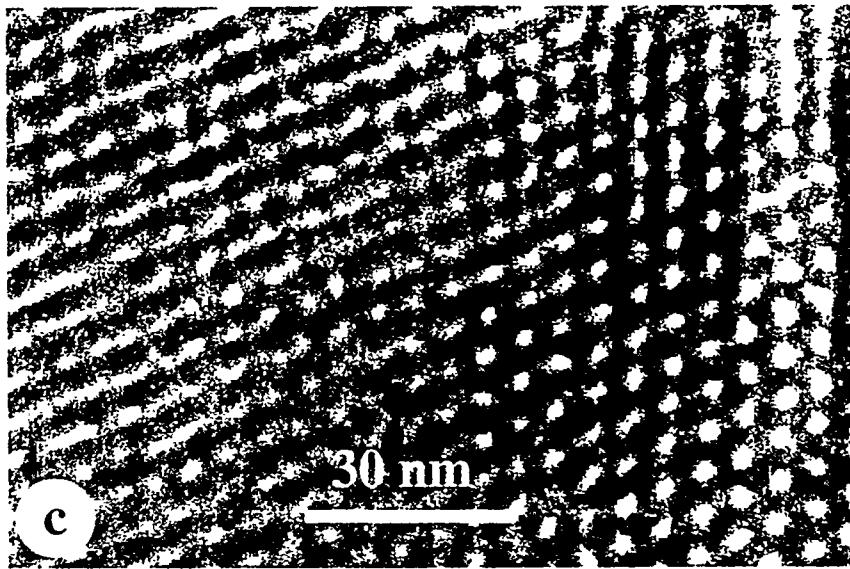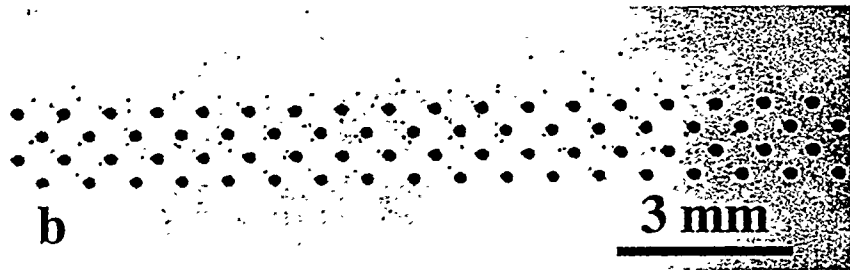30 nm
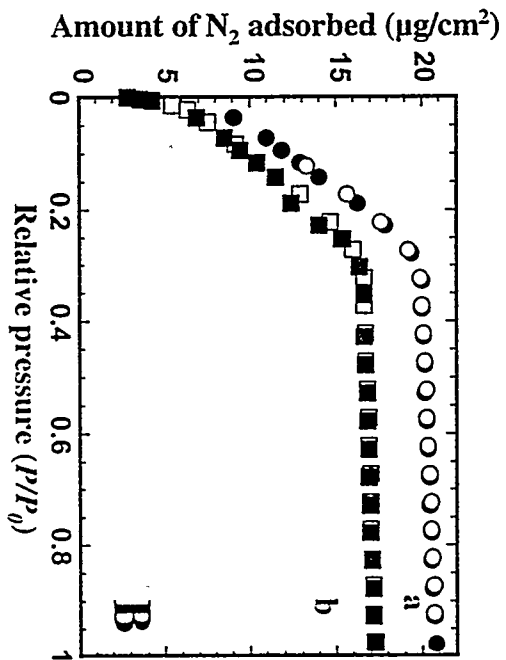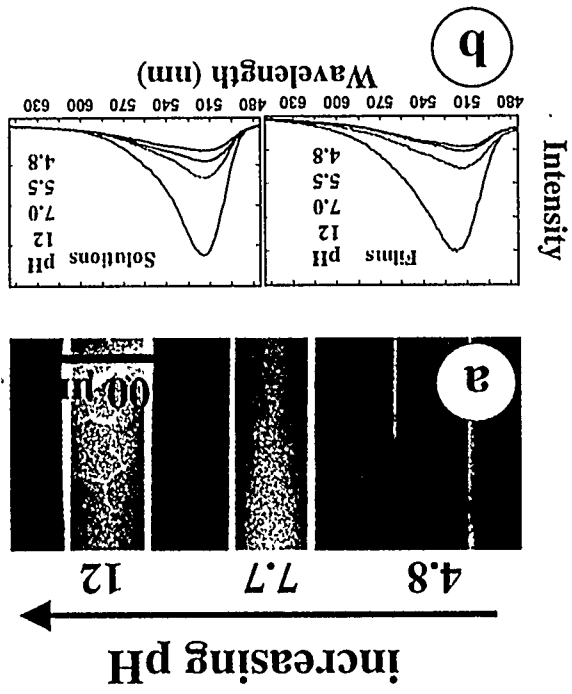
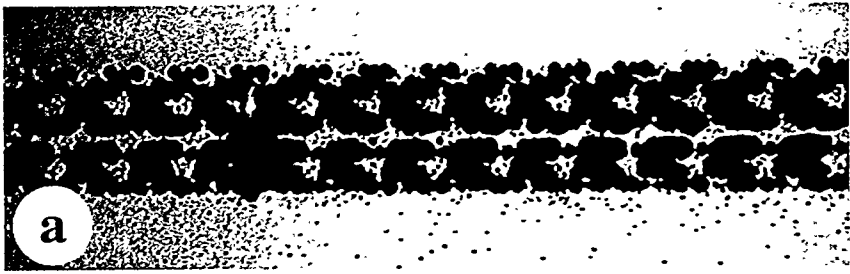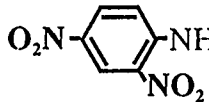Figure 5

Table 1. Functional organosilanes and properties of resultant thin film mesophases

	Functional Silanes[§]/additives [¶] R'-Si(OR)$_3$	Mesophase	Pore Size[*] (Å)	Surface Area[*] (m^2/g)	Properties and Applications
1	**F$_3$C(CF$_2$)$_5$CH$_2$CH$_2$Si(OC$_2$H$_5$)$_3$** Tridecafluoro-1,1,2,2-tetrahydrooctyltriethoxysilane (TFTS)	3-dH	25	850	Hydrophobic; low k dielectrics
2	**HS-(CH$_2$)$_3$Si(OCH$_3$)$_3$** Mercaptopropyltrimethoxysilane (MPS)	3-dH	25	1060	Coupling of noble metals
3	**NH$_2$-(CH$_2$)$_3$Si(OCH$_3$)$_3$** Aminopropyltrimethoxysilane (APS)	cubic	22	750	Coupling of noble metals, dye, and bioactive molecules
4	**Dye[#]-NH-(CH$_2$)$_3$Si(OCH$_3$)$_3$**	cubic	21	545	pH sensitive
5	**O$_2$N-⟨benzene ring⟩-NH(CH$_2$)$_3$Si(OC$_2$H$_5$)$_3$ NO$_2$**	3-dH	22	560	Chromophore; nonlinear optical material (χ^2)

[*]Pore size and surface area were determined from N$_2$ sorption isotherms obtained at −196°C, using a surface acoustic wave (SAW) technique[22]. Mass change due to nitrogen sorption was monitored (~80 pg.cm^{-2} sensitivity) as a function of nitrogen relative pressure. Pore size and surface area were determined from the isotherms using the BET equation and the BJH algorithm, respectively.

[§] Functional groups are retained through selective surfactant removal during heat treatment in nitrogen. TGA and DTA were used to establish the appropriate temperature window enabling complete surfactant removal without silane decomposition (H. Fan unpublished).

[¶] Additives investigated include rhodamine-B, cytochrome c (from Fluka), oil blue N, disperse yellow 3 (from Aldrich), silver ions and silver nanoparticles.

[#] Dye molecule used here is 5,6-carboxyfluorecein, succinimidyl ester (5,6-FAM, SE, from Molecular Probes).